Simulation of cracking phenomena during laser brazing of ceramics and cemented carbide

K. Nagatsuka*[1], Y. Sechi[2], N. Ma[3] and K. Nakata[1]

To investigate the mechanism of the occurrence of the microcracks produced in laser brazing of silicon carbide and cemented carbide using a silver–copper–titanium alloy as the filler metal, a numerical simulation for thermal cycle and thermal stress was performed using the finite element method. The laser-irradiated area of the cemented carbide was heated selectively, and almost uniform temperature distribution in the filler metal was obtained. The tensile thermal stress in the silicon carbide appeared near the interface between the silicon carbide and the filler metal, and the maximum principle stress at about 400 K during the cooling process reached the fracture strength of the silicon carbide. This resulted in the formation of microcracks in the silicon carbide which was observed in the experiment.

Keywords: Laser brazing, Microcrack, Silicon carbide, Active filler metal, Finite element method, Thermal stress

Introduction

Silicon carbide (SiC) has several functional characteristics, such as a low coefficient of thermal expansion (CTE); high thermal conductivity; good high temperature mechanical properties; superior wear, corrosion, heat, and oxidation resistances; and semiconducting properties. The dissimilar brazing of silicon carbide/metals using an active filler metal is a technique used commonly to produce cutting tools, ceramic heat exchangers, optical devices, and power devices.[1,2] The cemented carbides (WC–Co alloys) as classified into metal materials have low CTE and high rigidity, making them suitable for fabricating structural materials.[3] Thus, dissimilar joints of SiC/WC–Co alloys are ideal for forming cutting tools. However, certain problems remain with conventional brazing, such as material deterioration, the formation of a thick brittle compound layer, long treatment times and the occurrence of thermal stress–strain in the joint.[1,4] These problems arise because conventional furnace brazing requires long treatment times in order to ensure the heating and cooling of the whole component. On the other hand, laser brazing, in which a laser is used as the heat source, has attracted attention as a new method for forming dissimilar metal–metal joints as well as ceramics–metal joints.[5,6] In contrast to conventional furnace brazing, laser brazing can potentially minimise the growth of the brittle interfacial compound layer and prevent material deterioration, because the heating and cooling times in this process are short, only the selected part of the component needs to be heated, and the amount of heat input is small. In addition, this process uses less energy. Laser brazing has been performed at atmospheric pressure to form dissimilar metal–metal joints using a shielding inert gas. For instance, aluminium alloy–steel,[6] magnesium alloy–Ni-plated steel,[7] aluminium alloy–titanium alloy[8] joints have been formed using this technique. In addition, this technique has been brought into practical use in the automotive industry. As an instance of ceramics–metal joint, Huang *et al.*[9] have employed the dissimilar laser brazing to join diamond grits–steel substrate using a Cu–Ti–Sn metal powder as the filler in order to fabricate brazed diamond tools. Sudmeyer *et al.*[10] have reported the effect of surface patterning on the joint strength of laser brazed silicon carbide–steel joints formed using Ag–Cu–Ti and Sn–Ag–Ti as the filler metals. They found that the joint strength increased after surface patterning. In a previous study, we had used dissimilar laser brazing on ceramics such as sialon,[11] silicon carbide,[12] hexagonal boron nitride,[13] diamond,[14] and graphite,[15] while using a WC–Co alloy as the metal material. The effect of the active-element content of the filler metal on the joint strength and the interfacial reaction between the ceramics and the filler metal was investigated. However, little data is available on the stress and temperature distributions of joints formed by short dissimilar brazing process, such as laser brazing, has been reported.[16,17] The thermal stress during the cooling process caused by the mismatch in the CTE between ceramics and a filler metal, and between ceramics and a metal substrate often induces the occurrence of cracks in the brazed ceramics.[18,19] In addition, the temperature distribution and heating time also affect the diffusion of the active element, which is

[1]Joining and Welding Research Institute, Osaka University, Ibaraki, Osaka, Japan
[2]Kagoshima Prefectural Institute of Industrial Technology, Kagoshima, Japan
[3]JSOL Corporation, Tokyo, Japan

*Corresponding author, email nagatuka@jwri.osaka-u.ac.jp

Published by Maney on behalf of the Institute
Received 12 June 2014; accepted 4 August 2014
DOI 10.1179/1362171814Y.0000000241

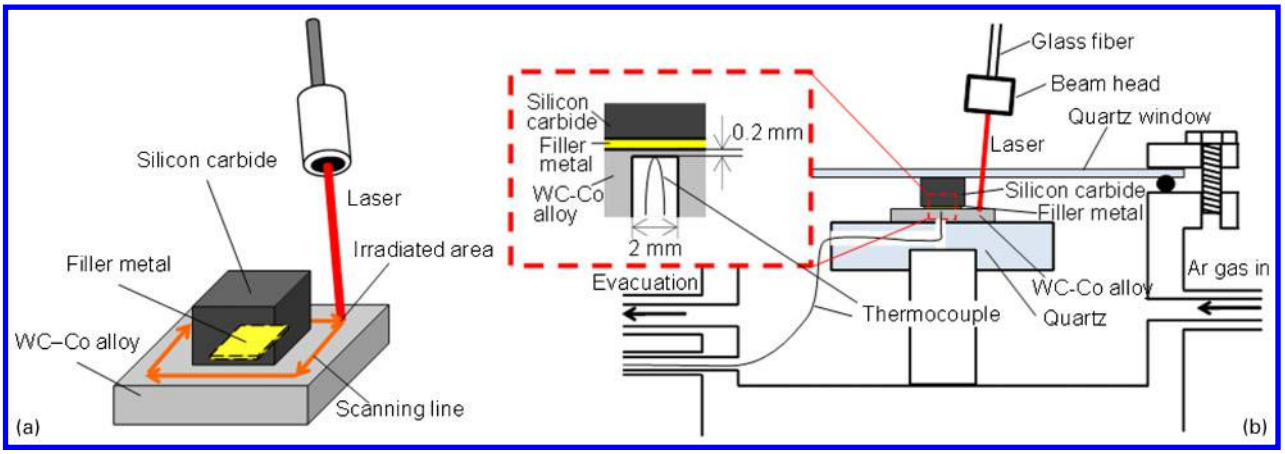

a image of laser heating; *b* cross-section of laser brazing apparatus

1 Schematic illustration of laser brazing

necessary for joining the ceramics. Therefore, in this study, we performed a numerical simulation of the thermal cycle and thermal stress during laser brazing of silicon carbide and a WC–Co alloy to investigate the mechanism of the occurrence of the cracks in the silicon carbide part of the laser brazed joint.

Laser brazing process

The experiments were performed using silicon carbide blocks, plates of the WC–Co alloy, and Ag–28Cu–1·7Ti (mass-%) filler metal sheets. The silicon carbide block was of recrystallised silicon carbide (>99 mass-% SiC, porosity of 17%) and had dimensions of $5 \times 5 \times 3{\cdot}5$ mm. The WC–Co alloy plate (ISO K10 grade) was used as the substrate; this had dimensions of $10 \times 10 \times 2$ mm. The thickness of the filler metal sheet was 0·1 mm, and its size was kept at 3×3 mm to ensure that it did not flow out of the joint interface. The dimensions and geometries of the materials used were designed based on a turning tool. For the temperature measurements, a WC–Co alloy plate with a hole was prepared by electric discharge machining. The hole was located at the middle in the square on the lower surface of the plate and had the diameter of 2 mm and the depth of 1·8 mm. Figure 1 shows a schematic illustration of the laser brazing process. The test specimen was shaped like a 'top hat'. A filler metal sheet was sandwiched between the silicon carbide block (placed above the sheet) and the WC–Co alloy plate (placed below the sheet) and placed in a vacuum chamber. The top of the specimen was covered with a transparent quartz glass plate, which not only acted as a window for the vacuum chamber during laser beam irradiation, but also fixed the specimen in place. The vacuum chamber was evacuated to less than 10^{-1} Pa, and Ar gas of 99·999% purity was pumped in until the pressure was equal to atmospheric pressure. This evacuation and substitution cycle was performed five times before brazing. During brazing, Ar gas was made to flow through the chamber at a rate of 5 L min^{-1}. Radiation from the yttrium aluminium garnet (YAG) and laser diode (LD) lasers was simultaneously transferred coaxially via optical fibres to the laser head unit, and was used to irradiate the sample through the transparent quartz glass plate on the top side of the WC–Co alloy plate at an irradiation angle of 85°. The LD laser was complemented the YAG laser in melting all of the filler metal. Table 1 lists the laser brazing conditions, which were set according to the standard JIS Z3261 BA-8 and the conditions used in previous studies.[12] The portion of the WC–Co alloy plate around the silicon carbide block was subjected to laser irradiation for 36 s. During laser heating, the temperature of the WC–Co alloy plate was monitored with an R-type thermocouple, which was inserted into the hole of the WC–Co alloy plate beneath the joint. The thermocouple was fixed at the middle in the square, and the distance between the thermocouple and the interface of the filler metal sheet/WC–Co alloy plate was 0·2 mm, as shown in Fig. 1*b*.

Numerical simulation analysis

Finite element model

A thermo-elastic–plastic analysis was performed using the finite element method to simulate the temperature and stress distributions induced by the laser brazing of silicon carbide and the WC–Co alloy using the Ag–Cu–Ti alloy as the filler metal. The explicit finite element method solver in LS-DYNA (version 971) was used.[20] Figure 2 shows the finite element model of laser brazing that was used. This model consisted of three parts (the silicon carbide block, the filler metal sheet, and the WC–Co alloy plate). The dimensions of these material components corresponded to those of the experimental specimens. The mesh size around the filler metal was $0{\cdot}1 \times 0{\cdot}1 \times 0{\cdot}1$ mm. The yellow line (beam element) indicates the heat input to the WC–Co alloy, and it moves around the silicon carbide block along the red line. The number of nodes and elements is 148 830 and 133 797, respectively. Table 2 lists the material properties,[21–25] and Fig. 3 shows the

Table 1 Laser-brazing conditions

Pulsed YAG average output/W	Pulsed YAG wave length/nm	CW LD output/W	CW LD wave length/nm	Pulse frequency/Hz	Scanning time/s	Atmosphere
134	1064	20	808	100	36	Ar flow (5 L min^{-1})

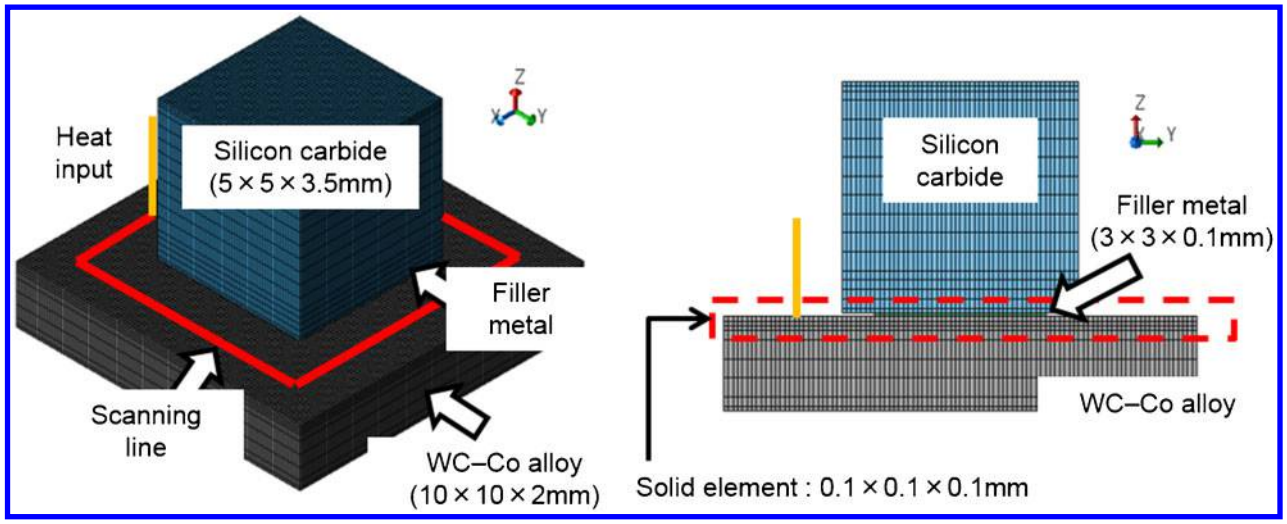

a specific heat; *b* thermal conductivity; *c* yield strength; *d* Young's modulus

2 Finite element model of laser brazing

temperature dependence of these properties for silicon carbide, the Ag–Cu–Ti filler metal, and the WC–Co alloy.[21–25] Because the silicon carbide is very brittle, its yield strength used in the simulation is almost equal to the fracture strength which is about a half of the bending strength based on experimental approximation.[26] A silicon carbide/filler metal/WC–Co alloy joint was formed after the laser heating in the experimental phenomena. In the simulation, the joined shape of silicon carbide/filler metal/WC–Co alloy was divided by finite element mesh, and then was heated by laser. Because the thermal stress in silicon carbide during heating would be very low, due to the low yield strength of the filler metal at high temperatures. In other word, the thermal stress induced in the silicon carbide during heating was released due to yield strength of the filler metal being low at high temperatures.

Boundary conditions

Fixing of WC–Co alloy

To prevent the spinning and parallel displacement of the model, the apexes at the bottom surface of the WC–Co alloy were fixed.

Heat input

The heat input was calculated as the mathematical product of the energy output of the YAG and LD lasers and their laser absorptivities.

The values of the laser absorptivity η were calculated using Bramson's formula[27,28]

$$\eta = 0{\cdot}365\left(\frac{R}{\lambda}\right)^{1/2} - 0{\cdot}0667\left(\frac{R}{\lambda}\right) + 0{\cdot}006\left(\frac{R}{\lambda}\right)^{3/2} \quad (1)$$

where R and λ are the electrical resistivity in Ω m (WC: 0·53 $\mu\Omega$ m) and the wavelength of the laser in m (YAG laser: 1064 nm, LD laser: 808 nm), respectively. The η values of the YAG and LD laser calculated by equation (1) were 0·23 and 0·26, respectively. Bramson's formula is only applicable for surface-oxide-layer-free metals specimen heated in vacuum. The presence of an oxide layer will increase the absorptivity.[28] However, this formula would be applicable for the laser brazing process, because the oxidation of WC was prevented by Ar gas flowing continuously in the chamber during laser heating.

Heat density distribution

A Gaussian distribution of the heat density in a half sphere was used in the thermal conduction simulation[20]

$$q = \frac{6 \times 3^{1/2} Q}{\pi \cdot \pi^{1/2} a^3} e^{\left(\frac{-3x^2}{a^2}\right)\left(\frac{-3y^2}{a^2}\right)\left(\frac{-3z^2}{a^2}\right)} \quad (2)$$

where q is the heat density at (x, y, z), Q is the net heat input from laser power, and a is the radius of the heating zone (a=0·2 mm).

Movement of heat source

The yellow line (beam element) is where the heat input to the WC–Co alloy. The heat was then transferred along the red square, which had sides of 7 mm, as shown in Fig. 2. The moving speed was 0·778 mm s^{-1}. Thus, the heating time was 36 s.

Heat transfer and radiation

The heated joint was cooled by the heat convection to the flowing Ar gas (5 L min^{-1}) and through heat

Table 2 Material properties of silicon carbide, Ag–Cu–Ti filler metal and WC–Co alloy[21–25]

	Density/ × 10^3 kg m^{-3}	Melting temperature /K	Specific heat*/J K^{-1} kg^{-1}	Thermal conductivity* /J s^{-1} m^{-1} K^{-1}	Coefficient of thermal expansion/ × 10^{-6} K^{-1}	Young's modulus*/ GPa	Yield strength*/ MPa
Silicon carbide	2·7	3003	700	50	4·5	80	50†
Filler metal	9·0	1063	114	219	19·6	83	272
WC–Co alloy	14·9	…	224	143	5·0	640	5230

*Temperature dependence.
†Fracture strength.

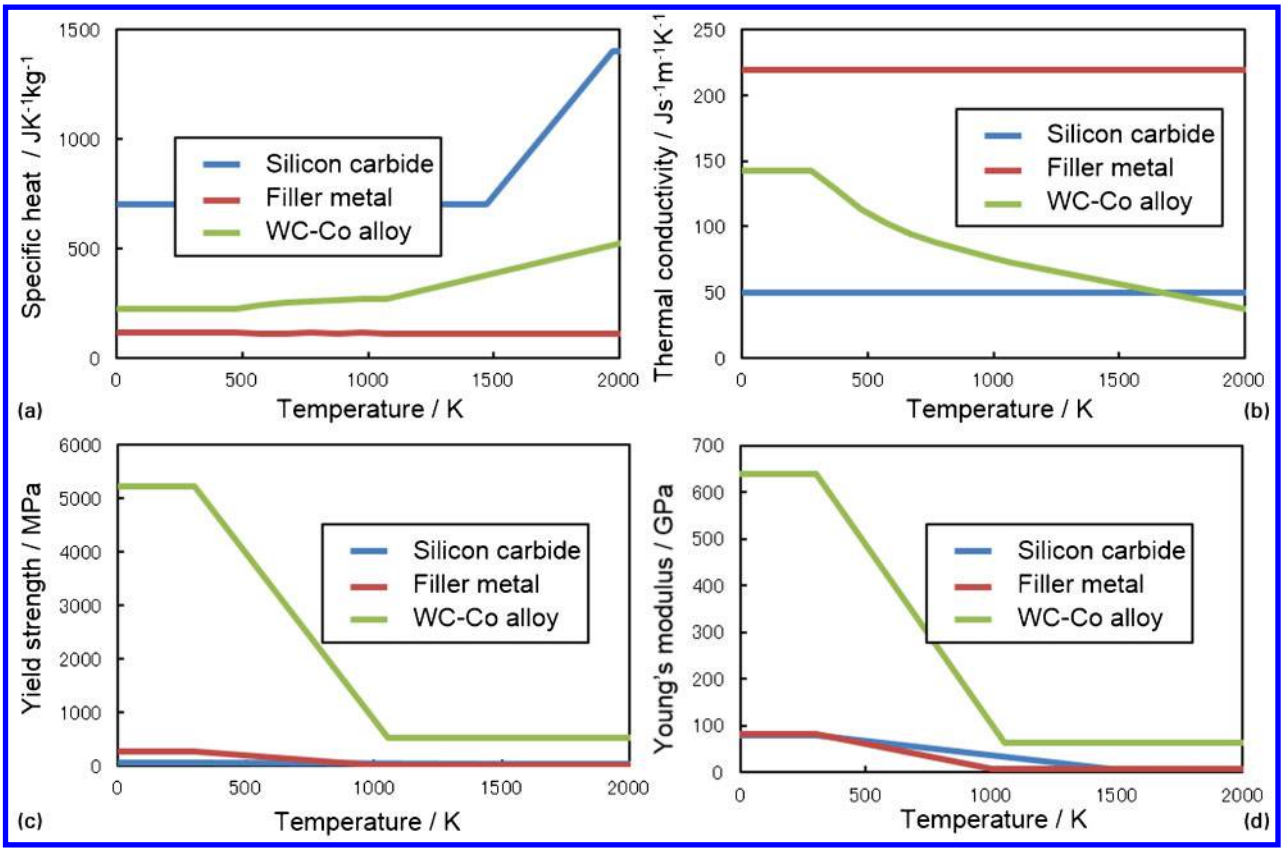

a appearance; *b* cross-section

3 Temperature-dependent material properties of silicon carbide, Ag–Cu–Ti filler metal and WC–Co alloy

radiation. The heat lost by the convection and that by the radiation were calculated together by the following simplified equation[20]

$$q_c = h(T_c - T_s) \tag{3}$$

where q_c, h, T_c, and T_s are the cooling heat flux, the coefficient of heat transfer between the environment within the chamber and the surface of the joint, the temperature of the environment (293 K), and the surface temperature of the joint, respectively. Figure 4 shows the temperature dependence of the heat-transfer coefficient.

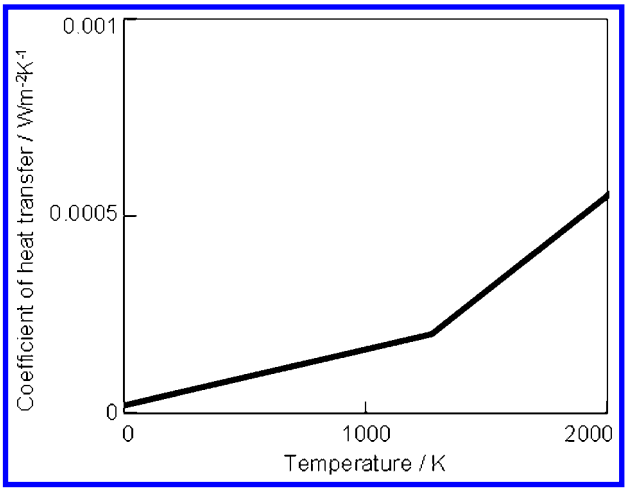

4 Temperature dependence of heat-transfer coefficient between environment inside of chamber and surface of joint

Results and discussion

Appearance and microstructure of brazed joint

Figure 5*a* and *b* shows the appearance and the cross-sectional microstructure of the laser-brazed joint repetitively. The laser irradiated area was observed on the WC–Co alloy around the silicon carbide block. Although no macrocrack was found on the brazed silicon carbide, a microcrack was observed in the silicon carbide block near the edge of the brazed filler metal. The mechanism of the microcrack occurrence was discussed based on the simulation results as bellows.

Temperature change during laser brazing

Figure 6 shows the measured and computed temperature changes in the WC–Co alloy during laser brazing. The temperature measurement was carried out in the hole which was located at the middle in the square on the lower surface of the WC–Co alloy plate and had the diameter of 2 mm and the depth of 1·8 mm. The distance between the measuring point and the filler metal/WC–Co alloy interface was 0·2 mm, and the position at which the temperature was computed corresponding to the measured position. The temperature increased rapidly after the laser irradiation. The maximum measured temperature was 1099 K, in contrast to the highest computed temperature, which was 1082 K. A margin of error of approximately ± 10 K in the maximum measured temperature was observed over three measurements. After laser irradiation, the temperature of the joint decreased. There was a good agreement between the measured and computed heating and cooling curves. The simulation model and the accuracy were verified.

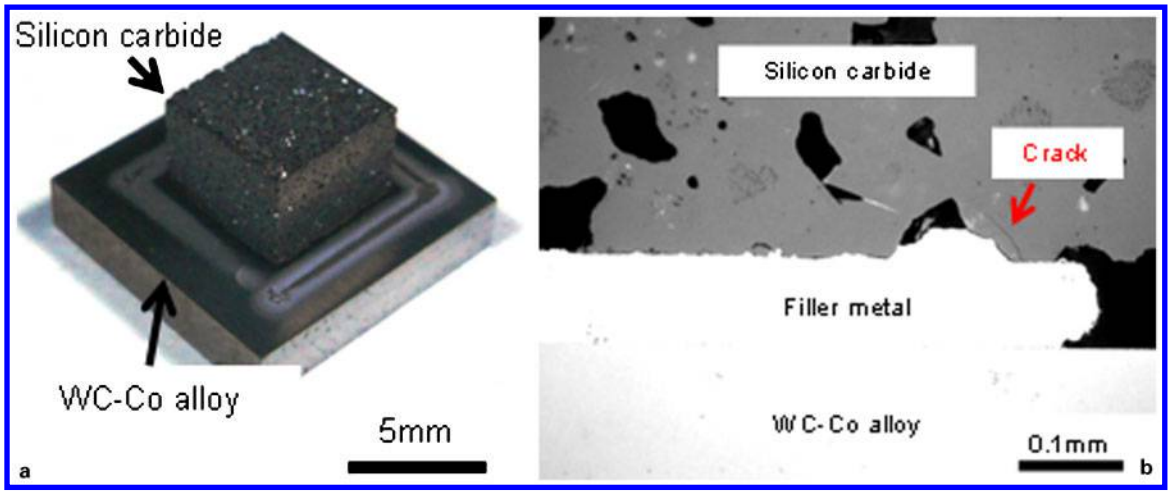

5 ***a*** **appearance and** ***b*** **cross-sectional microstructure of laser brazed joint**

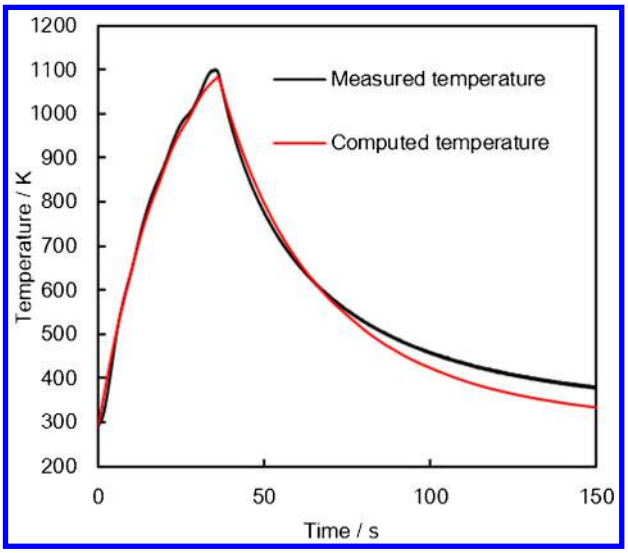

6 Measured and computed temperature changes in WC–Co alloy during laser brazing

Figure 7 shows the computed temperature distribution before (0 s), during (9, 18, 27 and 36 s), and after (300 s) the laser irradiation of the filler metal at the WC–Co alloy surface. The broken lines represent the silicon carbide block. When laser irradiation was completed at 36 s, the temperature reached the highest one. The difference in the temperature on the filler metal at various locations was smaller than 50 K during the laser irradiation and cooling process. In other words, although the laser irradiated area of the WC–Co alloy was selectively heated during laser irradiation, the temperature distribution of the filler metal became approximately uniform during heating and cooling in spite of the selective laser heating. These results proved that a uniform brazed joint can be successfully obtained by proposed selective laser heating. The entire filler metal component was heated to a temperature higher than the melting point of the filler metal (1063 K). The brazed joint was cooled to approximately the room temperature (293 K) after 300 s.

Stress distribution and microstructure of brazed joint

Figure 8 shows the distribution of the maximum principal stress (residual stress) on the brazed side of

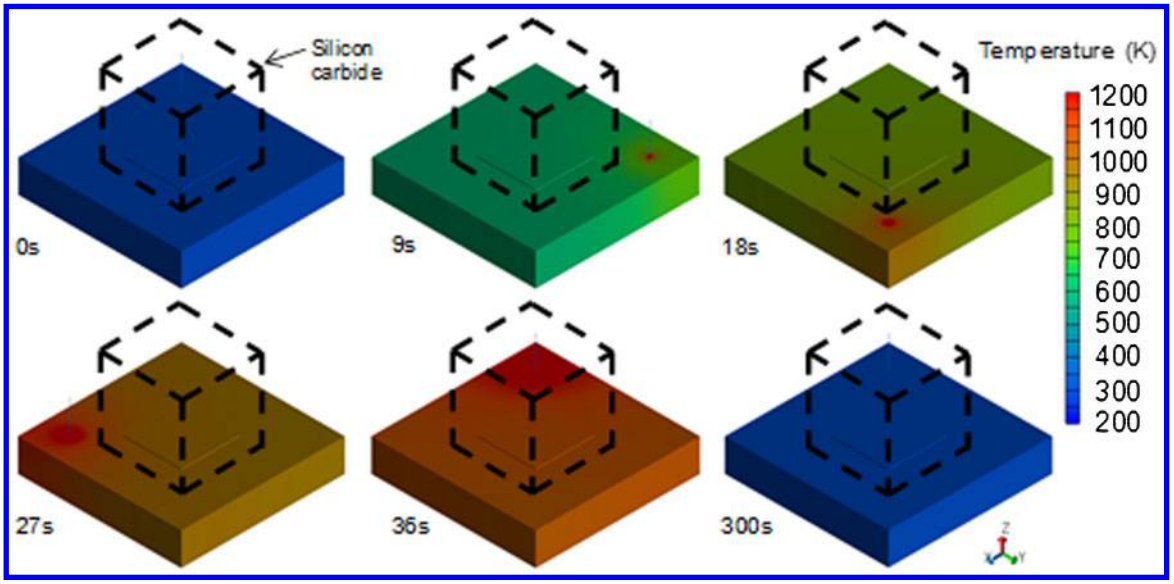

7 Computed temperature distribution before (0 s), during (9, 18, 27, and 36 s), and after (300 s) laser irradiation of filler metal and WC–Co alloy surface

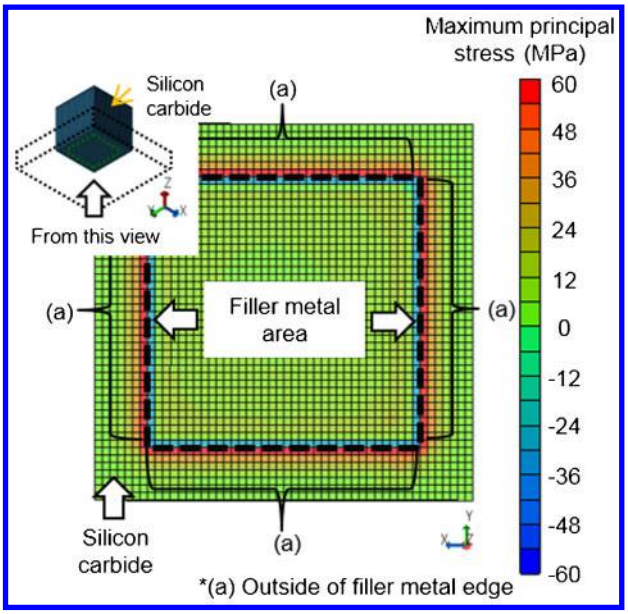

8 Maximum principal stress (residual stress) distribution on brazed side of silicon carbide after cooling

the silicon carbide block after cooling. It is known that knowing the maximum principal stress is essential for studying crack formation and fracture in brittle materials, such as ceramics.[29,30] The largest tensile maximum principal stress exceeding the fracture strength of silicon carbide (50 MPa) arose outside the brazed filler metal edge. Figure 9 shows the X, Y and Z axis stress (residual stresses) distributions of an X–Z cross-section around the brazed filler metal after cooling. The tensile stress was concentrated in the silicon carbide block outside the brazed filler metal edge (at position (1) in Fig. 9). The X axis stress was the largest among all the stresses within this X–Z cross-section. Figure 10 shows the relationship between the temperature and the X axis stress at position (1), which is shown in Fig. 9. The X axis stress increased with a decrease in the temperature during the cooling process, and reached the fracture strength of silicon carbide at approximately 400 K. This large tensile thermal stress was presumably caused by the mismatch between the CTE of the filler metal and that of silicon carbide. The CTE of silicon carbide used is $4{\cdot}5\times10^{-6}$ K^{-1}, that of the filler metal used is $19{\cdot}6\times10^{-6}$ K^{-1}, and that of the WC–Co alloy used is $5{\cdot}0\times10^{-6}$ K^{-1}. Thus, the CTE of the filler metal is four times those of silicon carbide and the WC–Co alloy. The filler metal expanded during heating and contracted during cooling. However, the contraction of the filler metal was restricted by the silicon carbide and the WC–Co alloy because these materials formed a joint. Therefore, the tensile stress in the filler metal and the compressive stress in the silicon carbide and the WC–Co alloy within the area where the silicon carbide and the WC–Co alloy were in contact with the filler metal arose as the thermal stress. As a result, the tensile thermal stress in the silicon carbide and the WC–Co alloy around the filler metal outside the contact area also arose due to the equilibrium force of the compressive stress. The position where the largest tensile thermal stress occurred corresponded to the position where the crack was formed, as can be seen from Fig. 5. Thus, the microcrack was caused by the thermal stress due to the mismatch in the CTEs of silicon carbide and the Ag–28Cu–1·7Ti (mass-%) filler metal. On the basis of this computation model, in our future studies, the possibility and effectiveness of thermal stress reduction methods can be investigated by changing the composition and the thickness of the filler metal. Furthermore, the laser power and the laser scanning patterns of this dissimilar joining process can be optimised for the high efficient production.

Conclusions

A numerical simulation of the temperature and stress distributions of a brazed joint of silicon carbide/silver–28 mass-% copper–1·7 mass-% titanium filler metal/cemented carbide was performed, and these results were compared with those of brazing experiments. The following conclusions were obtained.

1. There was a good agreement between the measured and computed heating and cooling curves. Based on the

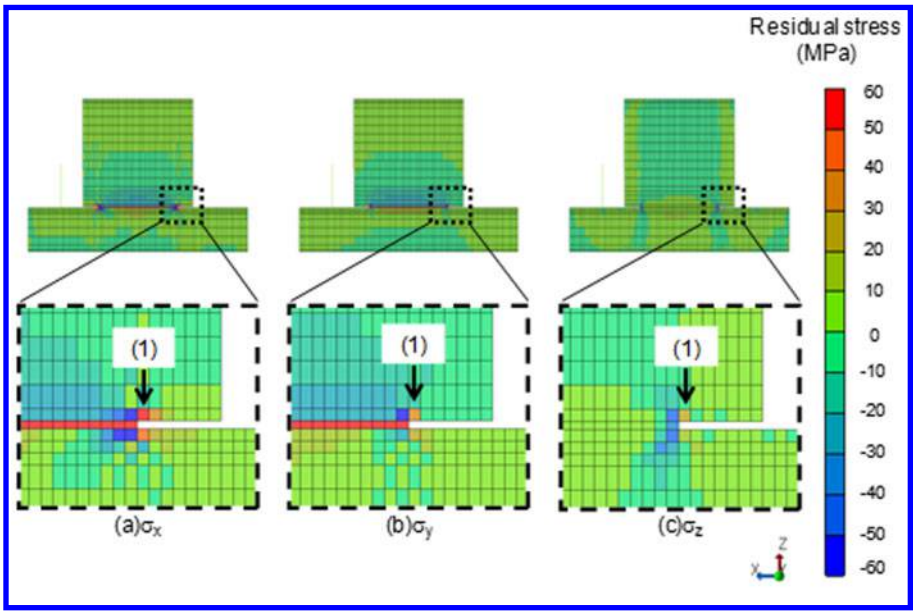

9 X, Y and Z axis stress (residual stress) distributions on X–Z cross-section around brazed filler metal after cooling

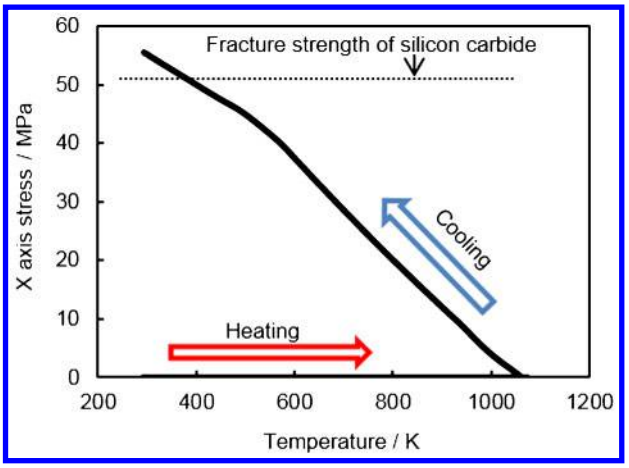

10 Relation between temperature and X axis stress at position (1) shown in Fig. 9

results of the thermal conduction analysis, although the laser-irradiated area of the cemented carbide was selectively heated during laser irradiation, the temperature distribution of the filler metal became approximately uniform during heating and cooling in spite of the selective laser heating.

2. A large tensile thermal stress induced by the laser brazing, reached the fracture strength of the silicon carbide at about 400 K during cooling. The largest stress arose in the silicon carbide outside the brazed filler metal area. This tensile thermal stress caused the formation of a microcrack in the silicon carbide block on the brazed joint.

References

1. Y. Liu, Z. R. Huang and X. J. Liu: 'Joining of sintered silicon carbide using ternary Ag-Cu-Ti active brazing alloy', *Ceram. Int.*, 2009, **35**, 3479–3484.
2. H. Chin, K. Cheong and A. Ismail: 'A review on die attach materials for SiC-based high-temperature power devices', *Met. Mater. Trans. B*, 2010, **41B**, 824–831.
3. W. J. Choyke, B. D'Urso, F. Yan and R. P. Devaty: 'Ultra-precision machining of stainless steel and nickel with single crystal 4H and 6H Boule SiC', *Mater. Sci. Forum*, 2010, **645–648**, 853–856.
4. H. Xiong, W. Mao, Y. Xie, W. Guo, X. Li and Y. Cheng: 'Brazing of SiC to a wrought nickel-based superalloy using CoFeNi(Si, B)CrTi filler metal', *Mater. Lett.*, 2007, **61**, 4662–4665.
5. Y. Sechi, T. Tsumura and K. Nakata: 'Dissimilar laser brazing of boron nitride and tungsten carbide', *Mater. Des.*, 2010, **31**, 2071–2077.
6. K. Saida, H. Ohnishi and K. Nishimoto: 'Fluxless laser brazing of aluminium alloy to galvanized steel using a tandem beam – dissimilar laser brazing of aluminium alloy and steels', *Weld. Int.*, 2008, **26**, 235–241.
7. A. M. Nasiri, P. Chartrand, D. C. Weckman and N. Y. Zhou: 'Thermochemical analysis of phases formed at the interface of a Mg alloy-Ni-plated steel joint during laser brazing', *Metall. Mater. Trans. A*, 2013, **44A**, 1937–1946.
8. S. Chen, L. Li, Y. Chen, J. Dai and J. Huang: 'Improving interfacial reaction nonhomogeneity during laser welding–brazing aluminum to titanium', *Mater. Des.*, 2011, **32**, 4408–4416.
9. S. F. Huang, H. L. Tsai and S. T. Lin: 'Laser brazing of diamond grits using a Cu–15Ti–10Sn brazing alloy', *Mater. Trans.*, 2002, **43**, 2604–2608.
10. I. Sudmeyer, T. Hettesheimer and M. Rohde: 'On the shear strength of laser brazed SiC–steel joints: effects of braze metal fillers and surface patterning', *Ceram. Int.*, 2010, **36**, 1083–1090.
11. K. Nagatsuka, S. Yoshida, Y. Sechi and K. Nakata: 'Effect of Ti content in Ag–Cu–Ti activated filler metal on dissimilar joint formation of sialon and WC–Co alloy by laser brazing', *Sci. Technol. Weld. Join.*, 2014, **19**, 521–526.
12. K. Nagatsuka, Y. Sechi and K. Nakata: 'Dissimilar joint characteristics of SiC and WC-Co alloy by laser brazing', *J. Phys. Conf. Series*, 2012, **379**, 012047, 1–9.
13. Y. Sechi, A. Takezaki, T. Matsumoto, T. Tsumura and K. Nakata: 'Composition dependence of titanium in silver-copper-titanium alloy braze on dissimilar laser brazing of boron nitride ceramics and cemented carbide', *Mater. Trans.*, 2009, **50**, 1294–1299.
14. Y. Sechi and K. Nakata: 'Dissimilar laser brazing of single crystal diamond and tungsten carbide', *Trans. JWRI*, 2012, **39**, 340–341.
15. K. Nagatsuka, Y. Sechi, Y. Miyamoto and K. Nakata: 'Characteristics of dissimilar laser-brazed joints of isotropic graphite to WC–Co alloy', *Mater. Sci. Eng. B*, 2012, **B177**, 520–523.
16. Z. Yang, L. Zhang, P. Luo and J. Xu: 'Finite element analysis on temperature field of laser brazing', *Adv. Mater. Res.*, 2011, **295–297**, 1428–1432.
17. Z. Yang and P. Luo: 'Finite element analysis on residual stress of laser brazing diamond wheel', *Adv. Mater. Res.*, 2013, **712–715**, 739–742.
18. S. Y. Kweon and S. K. Choi: 'Prediction of residual stress-induced cracking by finite element analysis', *Scr. Met.*, 1995, **32**, 359–364.
19. V. Cazajus, B. Lorrain, H. Welemane and M. Karama: 'Residual stresses in ceramic metal assembly after brazing process', *Adv. Sci. Technol.*, 2006, **45**, 1543–1550.
20. JSOL Corporation (ed.): 'LS-DYNA v.971 user manual 2nd edition'; 2011, Tokyo, JSOL Corporation.
21. J. Z. Wang, C. Yang, M. Chen and Z. Y. Guo: 'Molecular dynamics simulations of the heat capacity of Cu-Ag alloy', *J. Eng. Thermophys.*, 2002, **23**, 274–276.
22. I. Sudmeyer and M. Rohde: 'Investigations on the wetting and joining behavior of Ag-based braze fillers on silicon carbide', *Proc. SPIE*, 2008, **6880**, (68800J), 1–6.
23. E. Takegoshi, Y. Hirasawa and S. Imura: 'Experimental study on thermal properties of WC–Co sintered alloys', *Bull. Fac. Eng., Toyama Univ.*, 1984, **35**, 14–22.
24. S. Okamoto, K. Ohtuka, Y. Nakazono, Y. Shimoitani and J. Takada: 'Influence of WC grain size and Co mass content on mechanical properties of WC-Co cemented carbides', *J. Soc. Mater. Sci. Jpn*, 2005, **54**, 447–452.
25. The Japan Institute of Metals and Materials (ed.): 'Metals data book 3rd Ed'; 1995, Tokyo, Maruzen, Co., Ltd.
26. A. Xian and Z. Si: 'Direct comparison between tensile strength and flexural strength of ceramic/metal brazing joint', *Chin. J. Met. Sci. Technol.*, 1992, **8**, (1), 30–34.
27. P. X. Xu, C. M. Bao, F. G. Lu, C. W. Ma, J. P. He, H. C. Cui and S. L. Yang: 'Numerical simulation of laser–tungsten inert arc deep penetration welding between WC–Co cemented carbide and invar alloys', *Int. J. Adv. Manuf. Technol.*, 2011, **53**, 1049–1062.
28. M. Bass (ed.): 'Laser materials processing, materials processing theory and practices, Volume 3', 125; 1983, New York, North-Holland Publishing Company.
29. M. Galli, J. Botsis, J. Janczak-Rusch, G. Maier and U. Welzel: 'Characterization of the residual stresses and strength of ceramic-metal braze joints', *J. Eng. Mater. Technol.*, 2009, **131**, 0210004, 1–8.
30. Y. Zhou, F. H. Bao, J. L. Ren and T. H. North: 'Interlayer selection and thermal stresses in brazed Si_3N_4-steel joints', *Mater. Sci. Technol.*, 1991, **7**, 863–868.